AIAA JOURNAL
Vol. 42, No. 7, July 2004

Implementation of k–ω Turbulence Models in an Implicit Multigrid Method

Soo Hyung Park* and Jang Hyuk Kwon†
Korea Advanced Institute of Science and Technology, Daejeon 305-701, Republic of Korea

Three k–ω turbulence models using linear and nonlinear eddy-viscosity formulations are implemented in an implicit multigrid method. Detailed techniques of implementation are presented and discussed. Freezing and limiting strategies are applied to improve robustness and convergence of the multigrid method. The Wilcox k–ω, k–ω shear-stress transport, and Wilcox–Durbin+ (WD+) models are first tested for flat-plate flow, and the results are in good agreement with the empirical correlations. Numerical results for unseparated and separated transonic flows show that the WD+ model using weakly nonlinear eddy viscosity is in better overall agreement with the experimental data. Particularly for the separated flows, the present multigrid diagonalized alternating-direction implicit method provides good convergence without any robustness problems.

Introduction

SINCE Kolmogorov[1] proposed the first two-equation turbulence model using the specific dissipation rate ω, a number of two-equation turbulence models based on the ω equation have been proposed.[2,3] Wilcox[4] analyzed the k–ω model and established the closure coefficients of the model. His model gives excellent results for zero-gradient boundary-layer problems. Despite favorable numerical aspects, however, it suffers from freestream dependence. General k–ϵ models, conversely, do not suffer from this dependence.[5] Menter[6] therefore combined the k–ω model in the near-wall region and the k–ϵ model outside of the boundary layer into a single model. This model is known as the shear-stress transport (SST) model because it uses a weakly nonlinear eddy-viscosity formulation that considers the transport of principal turbulent shear stress in adverse pressure gradients.[7]

Recently, nonlinearity in eddy viscosity[8] has been reconsidered in view of realizability,[9] which is not satisfied by any linear eddy-viscosity formulation based on Boussinesq's assumption. Several researchers[10–12] have pointed out that the realizability condition could be fulfilled by decreasing the eddy viscosity. It was found that weakly nonlinear eddy-viscosity formulations improve the performance of turbulence models for flows in the presence of adverse pressure gradients, particularly in shockwave/boundary-layer interactions.[13] In this study, Wilcox's k–ω,[4] Menter's k–ω SST,[6] and the weakly nonlinear Wilcox–Durbin (WD+) models[13] are implemented to examine their performance for two- and three-dimensional transonic flows.

An important requirement in solving the turbulent Navier–Stokes equations is the robustness and efficiency of the solution method. Two-equation turbulence models inevitably have stiff source terms and use very small grid size to resolve the thin boundary layer in high-Reynolds-number flows. This may cause difficulties in stability and convergence, and several studies using the multigrid method[14] have been conducted in an effort to accelerate the convergence of two-equation turbulence models.[15–17] Some difficulties, however, remain in implementation of the multigrid method with respect to the turbulence transport equations. To stabilize the computations one may solve the turbulence transport equations only on the finest grid. However, this may cause slowdown of convergence rates because of a disparity between flow and turbulence variables as the multigrid level increases. To improve the convergence rate with a multigrid, it is important to solve the turbulence transport equations on coarser grids. Next, care is needed in the limiting process to preserve the positivity of k and ω. Even though implicit treatment of stiff source terms guarantees positivity of the turbulence variables under certain conditions, the numerical conditions may lead to unphysical values in the turbulence variables. In this work, the eddy viscosity and production terms are frozen in coarser grids by passing down the values without a new calculation.[17] Necessary limits are also introduced to avoid these situations.

Turbulent flat-plate flow is first computed and a grid refinement study is performed in order to evaluate the turbulence models. To demonstrate the efficiency of the present algorithm, the transonic flows past the RAE2822 airfoil and the three-dimensional ONERA-M6 wing are computed and compared with experimental data.

Governing Equations

In the present work, the compressible Navier–Stokes equations and the k–ω turbulence equations are considered.

The Navier–Stokes equations are

$$\frac{\partial \boldsymbol{q}}{\partial t} + \frac{(\partial \boldsymbol{f}_j - \boldsymbol{f}_{vj})}{\partial x_j} = 0 \tag{1}$$

where $\boldsymbol{q}$ is the flow variable and $\boldsymbol{f}_j$ and $\boldsymbol{f}_{vj}$ are the inviscid and viscous fluxes in each direction,

$$\boldsymbol{q} = \begin{bmatrix} \rho \\ \rho u_i \\ \rho E \end{bmatrix}, \qquad \boldsymbol{f}_j = \begin{bmatrix} \rho u_j \\ \rho u_j u_i + p\delta_{ij} \\ \rho u_j H \end{bmatrix} \tag{2}$$

$$\boldsymbol{f}_{vj} = \begin{bmatrix} 0 \\ \tau_{ij} + \tau^*_{ij} \\ u_j\left(\tau_{ij} + \tau^*_{ij}\right) - q_j + (\mu_l + \sigma_k \mu_t)\dfrac{\partial k}{\partial x_j} \end{bmatrix} \tag{3}$$

Here ρ and p are the density and pressure, u_j are the Cartesian velocity components, E is the total energy, and $H = E + p/\rho$ is the total enthalpy. The quantity τ_{ij} and τ^*_{ij} are the laminar and turbulent stresses, respectively, and q_j are the heat fluxes in each direction, which are defined as

$$\tau_{ij} = 2\mu_l\left(S_{ij} - \frac{1}{3}S_{kk}\delta_{ij}\right) \tag{4}$$

Received 15 May 2003; revision received 12 January 2004; accepted for publication 19 February 2004.

*Postdoctoral Researcher, Department of Aerospace Engineering. Member AIAA.

†Professor, Department of Aerospace Engineering, 373-1 Guseong-dong, Yuseong-gu. Senior Member AIAA.

$$\tau_{ij}^{*} = 2\mu_t\left(S_{ij} - \frac{1}{3}S_{kk}\delta_{ij}\right) - \frac{2}{3}\rho k\delta_{ij} \tag{5}$$

$$q_j = -\frac{\gamma R}{\gamma - 1}\left(\frac{\mu_l}{Pr_l} + \frac{\mu_t}{Pr_t}\right)\frac{\partial}{\partial x_j}\left(\frac{p}{\rho}\right) \tag{6}$$

where γ is the ratio of specific heats and R is the gas constant. The variables Pr_l and Pr_t are the laminar and turbulent Prandtl numbers, respectively. The quantity μ_l is the molecular viscosity determined by the Sutherland law and μ_t is the eddy viscosity, which is defined later. The S_{ij} are the velocity strain rates:

$$S_{ij} = \frac{1}{2}\left(\frac{\partial u_i}{\partial x_j} + \frac{\partial u_j}{\partial x_i}\right) \tag{7}$$

The k–ω equations can be written as

$$\frac{\partial \boldsymbol{q}_T}{\partial t} + \frac{\left(\partial \boldsymbol{f}_{T_j} - \boldsymbol{f}_{T_{vj}}\right)}{\partial x_j} = \boldsymbol{S}_{k\omega} \tag{8}$$

where $\boldsymbol{q}_T = [\rho k, \rho\omega]^T$ and the convection and diffusion terms of the turbulent equations are expressed as

$$\boldsymbol{f}_{T_j} = \begin{bmatrix}\rho u_j k \\ \rho u_j \omega\end{bmatrix}, \qquad \boldsymbol{f}_{T_{vj}} = \begin{bmatrix}(\mu_l + \sigma_k\mu_t)\dfrac{\partial k}{\partial x_j} \\ (\mu_l + \sigma_\omega\mu_t)\dfrac{\partial \omega}{\partial x_j}\end{bmatrix} \tag{9}$$

where $\boldsymbol{S}_{k\omega}$ is the turbulent source vector. The source vector is composed of the production rates of k and ω, denoted by P_k and P_ω, and their destruction rates, D_k and D_ω. The cross-diffusion term, denoted by P_{cd}, for the k–ω SST model is added to the ω equation. The eddy viscosity μ_t depends only on turbulent scales:

$$\mu_t = \rho\alpha_v c_\mu^o (k/\omega) \tag{10}$$

where α_v is defined by c_μ/c_μ^o and c_μ^o is a constant, 0.09.

Original k–ω Model[4]

The original model is

$$\boldsymbol{S}_{\mathrm{org}} = \begin{bmatrix}P_k - D_k \\ P_\omega - D_\omega\end{bmatrix} = \begin{bmatrix}\mu_t S^2 - \dfrac{2}{3}\rho k S_{kk} - \beta'\rho k\omega \\ \alpha\dfrac{\omega}{k}\left(\mu_t\dfrac{S^2}{\alpha_v} - \dfrac{2}{3}\rho k S_{kk}\right) - \beta\rho\omega^2\end{bmatrix} \tag{11}$$

where the mean strain rate is defined by

$$S^2 = 2S_{ij}S_{ji} - \tfrac{2}{3}S_{kk}^2 \tag{12}$$

The closure constants are $\sigma_k = \sigma_\omega = 0.5$, $\beta' = 1$, $\alpha = \frac{5}{9}$, and $\beta = \frac{5}{6}$. The original k–ω model uses a constant value of $\alpha_v = 1$ in the eddy viscosity:

$$\mu_t = \rho c_\mu^o (k/\omega) \tag{13}$$

The linear eddy-viscosity formulation of Eq. (13) was designed to predict the boundary-layer flows accurately with a zero pressure gradient.

The k–ω Wilcox–Durbin+ (WD+) Model[13]

The linear eddy viscosity is known to be inadequate in the presence of adverse pressure gradients. Bradshaw et al.[8] pointed out that the shear stress is proportional to the turbulent kinetic energy but not to the velocity gradient, in a two-dimensional boundary layer:

$$\tau_{ij}^{*} = -\rho\widetilde{uv} = \rho\sqrt{c_\mu^o}\,k \tag{14}$$

Both expressions of Eqs. (13) and (14) can be combined by a functional:

$$c_\mu = \min\left[c_\mu^o, \sqrt{c_\mu^o}\,\omega/S\right] \tag{15}$$

This combination was proposed by Coakley[7] and applied to the k–ω SST model[6] later. This weakly nonlinear correction is also fundamentally identical to Durbin's realizability correction[11]. The essential point of the correction is to produce asymptotic behavior of c_μ when the mean strain rate S tends toward infinity. More detailed discussion is found in Ref. 13. In this work, a more elaborate expression of c_μ is used to account for the three-dimensional effect[10]:

$$c_\mu = \min\left[c_\mu^o, \frac{\sqrt{c_\mu^o}\,\omega}{\sqrt{(S^2 + \Omega^2)/2}}\right] \tag{16}$$

where Ω is the absolute value of the vorticity and is defined by

$$\Omega^2 = \frac{1}{2}\left(\frac{\partial u_i}{\partial x_j} - \frac{\partial u_j}{\partial x_i}\right)^2 \tag{17}$$

If c_μ is set to c_μ^o, the source vector and closure constants of the WD+ model are the same as those of the Wilcox k–ω equations.

The k–ω Shear-Stress Transport (SST) Model[6]

The key concepts behind the SST model are retaining the robust and accurate formulation of the Wilcox k–ω model in the near-wall region and exploiting the freestream independence of the k–ϵ model in the outer part of the boundary layer[6]. To accomplish this, the k–ϵ model is transformed into a k–ω formulation. The differences between this formulation and the original k–ω formulation are that an additional cross-diffusion term appears in the ω equation and that the modeling constants are different. The closure constants in the original k–ω model (ϕ_1) and in the transformed k–ϵ model (ϕ_2) are blended by the following relation between them:

$$\phi = F_1\phi_1 + (1 - F_1)\phi_2 \tag{18}$$

where all constants (α, β, β', σ_k, σ_ω), as well as the function F_1, are given in Ref. 6.

The cross-diffusion term is added to the source vector of the ω equation as

$$P_{\mathrm{cd}} = 2\rho(1 - F_1)\frac{\sigma_{\omega 2}}{\omega}\frac{\partial k}{\partial x_j}\frac{\partial \omega}{\partial x_j} \tag{19}$$

For the k–ω SST model, the eddy-viscosity formulation was derived from the assumption of Bradshaw et al.[8] in the adverse-pressure-gradient region. The coefficient c_μ can be written as

$$c_\mu = \min\left[c_\mu^o, 0.31\omega/\Omega F_2\right] \tag{20}$$

where F_2 is a blending function that is designed to be 1 for boundary-layer flows and 0 for free shear layers. A difference in c_μ from the WD+ model is that the SST model adopts the absolute value of the vorticity Ω.

Numerical Methods

The governing equations in the physical coordinate system are transformed into computational coordinates and Eqs. (1) and (8) are discretized by the cell-centered finite volume method. Then the governing equations yield

$$\frac{\mathrm{d}\boldsymbol{Q}_{ijk}}{\mathrm{d}t} + \boldsymbol{R}_{ijk} = 0 \tag{21}$$

where $\boldsymbol{Q} = \boldsymbol{q}/J$ and J is the Jacobian of the coordinate transformation. The residual $\boldsymbol{R}_{ijk}$ consists of the inviscid and viscous parts of the numerical flux at the cell faces.

Spatial Discretization

The inviscid flux requires an artificial dissipation to prevent numerical instabilities around discontinuities. In this study, Roe flux-difference splitting and the third-order MUSCL are used with the van Albada limiter (see Ref. 18) to obtain second-order accuracy. Simple central differencing is applied to obtain variable gradients of the viscous flux. Although this simple differencing may cause an odd–even decoupling problem where oscillating or small-shear flows exist, the decoupling effects are not considered in this study.

A simple second-order upwind MUSCL method is applied to the k and ω equations without any limiter. This simple method was used by Liu and Zheng.[16] Although a limiter to suppress unwanted numerical oscillation is required in discretizing Navier–Stokes equations, it is not required for the k–ω equations. Numerical experiments have shown that the limiter for the k–ω equations often causes difficulty in convergence.

Diagonalized Alternating-Direction Implicit Method

The diagonalized alternating-direction implicit (DADI) method is applied to find steady-state solutions.[19–21] The ADI method is diagonalized using the local similarity transformation of the inviscid flux Jacobian:

$$\begin{aligned}\boldsymbol{T}_1\left\{\boldsymbol{I}/\Delta t+\nabla^-\Lambda_1^+ + \nabla^+\Lambda_1^- - \bar{\delta}_1^2 r(A_{v1})\right\}\boldsymbol{T}_1^{-1}\\ \cdot \boldsymbol{T}_2\left\{\boldsymbol{I}/\Delta t+\nabla^-\Lambda_2^+ + \nabla^+\Lambda_2^- - \bar{\delta}_2^2 r(A_{v2})\right\}\boldsymbol{T}_2^{-1}\\ \cdot \boldsymbol{T}_3\left\{\boldsymbol{I}/\Delta t+\nabla^-\Lambda_3^+ + \nabla^+\Lambda_3^- - \bar{\delta}_3^2 r(A_{v3})\right\}\boldsymbol{T}_3^{-1}\Delta\boldsymbol{Q}=-\boldsymbol{R}^n\end{aligned} \tag{22}$$

where $\boldsymbol{T}_i$ are the left eigenvector matrices of the flux Jacobian[19] and $\Lambda_i^{\pm}$ are the eigenvalues of the Navier–Stokes equations in each direction. Here, $\nabla^{\pm}$ denote the backward and forward difference operators and $\bar{\delta}_i^2 r(A_{vi})$ operators express the central differencing of viscous fluxes. It should be noted that the contribution of viscous terms is not simultaneously diagonalizable, in contrast to the inviscid one, and it is added in the implicit part only by an approximation of spectral radius scaling[20]:

$$r(A_v) = 2(\mu_l/\mathrm{Pr}_l + \mu_t/\mathrm{Pr}_t)(\gamma/\rho) \tag{23}$$

For a similar reason, local time stepping is applied to Δt, which is defined by Courant–Friedrichs–Lewy (CFL) over the summation of the spectral radii of the inviscid and viscous flux vectors. The solution procedure is similar to that of the block ADI scheme. Even with the additional matrix–vector products, the diagonalized algorithm is more efficient than the block algorithm.

A loosely coupled algorithm is used to integrate the Navier–Stokes and the k–ω equations separately. This approach has been widely used to implement most turbulence-model equations, although a fully coupled algorithm[16] would be faster than a loosely coupled one. For the loosely coupled algorithm, the convergence of k–ω equations may lag behind the Navier–Stokes equations and several algorithms have been devised because time lagging results in poor convergence of a loosely coupled system. Zheng and Liu[15] suggested multiple iterations of the k–ω equations for each time step of the Navier–Stokes equations. In the present loosely coupled implicit algorithm, the k–ω equations are marched only one time step for each Navier–Stokes iteration because more iterations do not reduce the total computing time for the implicit method.

For k–ω turbulence equations, the source vector of Eq. (11) must be treated implicitly because it results in a stiffness problem of the time-marching methods. While S^2 and P_{cd} terms are treated explicitly, the contributions of the turbulent dissipation terms D_k and D_ω are added in the implicit parts to increase the diagonal dominance.[16] Therefore, the approximate Jacobian of the source terms can be expressed as

$$\boldsymbol{W} = \frac{1}{J}\begin{bmatrix}-\max\left(0, \frac{2}{3}S_{kk}\right) - 2\beta'\omega & 0\\ 0 & -\max\left(0, \frac{2}{3}S_{kk}\right) - 2\beta\omega\end{bmatrix} \tag{24}$$

The resulting scheme for each turbulence equation becomes only a scalar ADI method if this DADI procedure is applied:

$$\begin{aligned}\left\{\boldsymbol{D}+\nabla^-\Lambda_1^+ + \nabla^+\Lambda_1^- - \bar{\delta}_1^2 r^t\left(A_{v_1}\right)\right\}\boldsymbol{D}^{-1}\\ \cdot\left\{\boldsymbol{D}+\nabla^-\Lambda_2^+ + \nabla^+\Lambda_2^- - \bar{\delta}_2^2 r^t\left(A_{v_2}\right)\right\}\boldsymbol{D}^{-1}\\ \cdot\left\{\boldsymbol{D}+\nabla^-\Lambda_3^+ + \nabla^+\Lambda_3^- - \bar{\delta}_3^2 r^t\left(A_{v_3}\right)\right\}\cdot\Delta\boldsymbol{Q}_{kw} = -\boldsymbol{R}_{kw}^n\end{aligned} \tag{25}$$

where the diagonal term $\boldsymbol{D}=\boldsymbol{I}/\Delta t - \boldsymbol{W}$. Equation (25) is marched with frozen flow variables immediately after Eq. (22) is solved. Time stepping different from that of the Navier–Stokes equations can be used because the estimated spectral radii are different from those of the Navier–Stokes equations:

$$r^t(A_v) = 2[(\mu_l + \sigma_k\mu_t)/\rho] \tag{26}$$

Although implicit treatment of the source term greatly improves the robustness involved with the positivity of the turbulence variables, the ω equation cannot preserve the positivity constantly. This causes an unphysically low level of ω, resulting in higher values of eddy viscosity μ_t. Following Zheng and Liu,[15] a lower limit for ω is imposed for every iteration after the turbulence equations are solved:

$$(\rho\omega)_{\min} = \alpha\rho S \tag{27}$$

Another difficulty in stability is that the solution method may allow the change of the turbulence variables to be much larger than the current value. Therefore, further limitation is necessary for the changes; this is accomplished with $\Delta(\rho k)$ and $\Delta(\rho\omega)$. After each implicit sweep, $\Delta(\rho k)$ and $\Delta(\rho\omega)$ are limited to one-half of their current values only if the sign of the changes is negative. Numerical experiments show that this limit effectively prevents k and ω from being negative in the initial transient stage.

Multigrid Algorithm

The acceleration mechanisms of the multigrid method are high-frequency damping improvement and fast wave propagation in coarser meshes.[14] In spite of its fairly good efficiency, the DADI algorithm has not been recommended in multigrid applications because the high-frequency damping characteristics are not very effective.[21] For this reason the present V-cycle multigrid algorithm concentrates on acceleration of wave propagation.[22] To this end, different numbers of time steps, as well as CFL numbers, are applied according to the grid level. We then let L be the grid level and $L=1$ for the finest level. In this work, two time steps are advanced at the coarse levels. In addition, the CFL, number is increased according to the grid level. When the CFL number of the finest level is CFL_1, that of the coarse levels is determined by $\mathrm{CFL}_L = \mathrm{CFL}_1\sqrt{(L)}$.

The multigrid method for the turbulence equations requires a careful approach because of their high stiffness, which arises from the nonlinear source terms. It has been noted that the accuracy of strongly nonlinear terms cannot be preserved at coarser levels because the velocity gradients can significantly alter the magnitude of the source terms. Thus it is important to freeze the nonlinear terms in order to preserve the turbulence variables of the coarse levels.[16,17] The S^2 and S_{kk} terms are calculated only on the finest grid and restricted as frozen values on the coarser grids:

$$(S^2)_{2h} = \Sigma V_h(S^2)_h \big/ V_{2h} \tag{28}$$

$$(S_{kk})_{2h} = \Sigma V_h(S_{kk})_h / V_{2h} \tag{29}$$

where V denotes the cell volume. In addition, the cross-diffusion term P_{cd} is restricted by the same volume-weighted averaging for the k–ω SST model. The eddy viscosity is also restricted in the same way. Freezing the eddy viscosity helps obtain robust convergence, particularly when freestream values are used for the initial conditions.

Another modification for the multigrid lies in the limiting process. The limit for ω, Eq. (27), is known to hinder the effectiveness

of the multigrid when it is directly imposed at every time step in coarse grids.[16] Our numerical experiments, however, show that direct imposition of the limit does not counteract the efficiency of the present implicit multigrid method. Therefore, the limit for ω is directly imposed on all grid levels in this study.

Boundary Conditions

The characteristic boundary conditions using the Riemann invariant are enforced for the subsonic inflow or outflow. The freestream ω is determined by using the following estimate proposed by Menter[5]:

$$\omega_\infty = \mathcal{O}[10(U_\infty/L)] \tag{30}$$

where U_∞ is the freestream velocity and L the characteristic length. The freestream eddy viscosity is set to 0.009 μ_l, and the turbulent kinetic energy is calculated from the definition of the eddy viscosity. It is well known that k–ω models have freestream dependence. This dependence is still present in the original k–ω and k–ω WD+ but it is not found in the k–ω SST model. Freestream dependence is not considered for the cases in this study because it is not important for the magnitude of the wall coefficients when the flows are wall-bounded and the far-field boundary is far away from the wall.[5]

At the solid walls, no-slip conditions for velocities are applied and the density and energy are extrapolated from the interior cells. The value of k is set to zero at the wall. Because the specific dissipation rate ω is theoretically infinite at the wall, it is often recommended that its asymptotic value be imposed at several interior points.[4,6] Although it has been thought to be important for solution accuracy, it creates difficulty in applying the turbulence model to complex flow fields. Following the approach in Ref. 16, the boundary value of ω can be specified only as

$$\omega_{\text{wall}} = (19/9)\left(6\mu_w \big/ \beta\rho d_1^2\right) \tag{31}$$

where d_1 is the distance of the first cell center from the wall. It is noted that this boundary condition using the distance to the first cell center may cause grid dependence. It may also degrade the convergence of the multigrid if different ω values are imposed in each multigrid level. In this study, a modified ω value at the wall is used to reduce the grid dependence and to improve the multigrid convergence:

$$\omega_{\text{wall}} = \text{CN}(19/9)\left(6\mu_w \big/ \beta\rho d_1^2\right) \tag{32}$$

where $\text{CN} = 0.1 \times \min[50, \max(10, Re_\infty d_1 - 20)]$ and $Re_\infty d_1$ is known as the cell Reynolds number (CRN). Note that CN is set to one for CRN of 30 below.

Numerical Results

Turbulent Boundary-Layer Flow over a Flat Plate

To verify the implementation of the turbulent models, a turbulent boundary layer over a flat plate is first presented. The freestream conditions are $M_\infty = 0.2$ and $Re = 10^7$, based on the plate length. The freestream turbulence intensity $2k/(3\rho_\infty U_\infty^2)$ is set to 10^{-4}. The grids employed to compute the turbulent boundary layer consist of 193×65 node points, with 25 points before the leading edge and

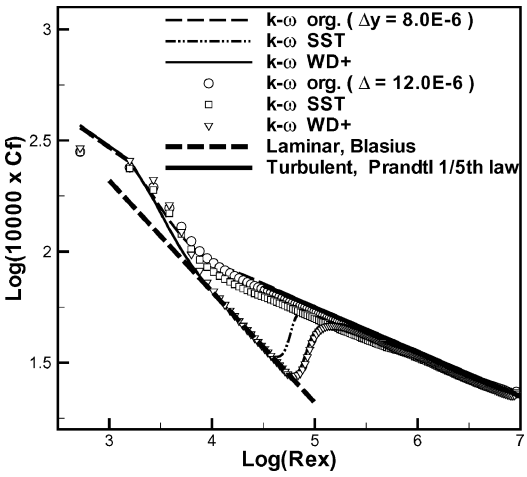

a) Skin friction coefficient

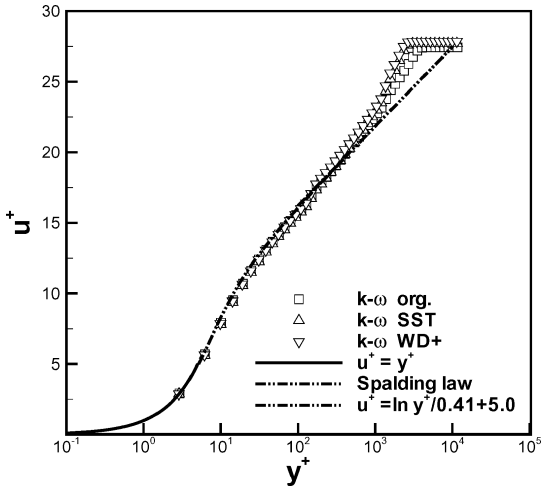

b) Velocity profile

Fig. 1 Solution with turbulence model using modified ω at wall.

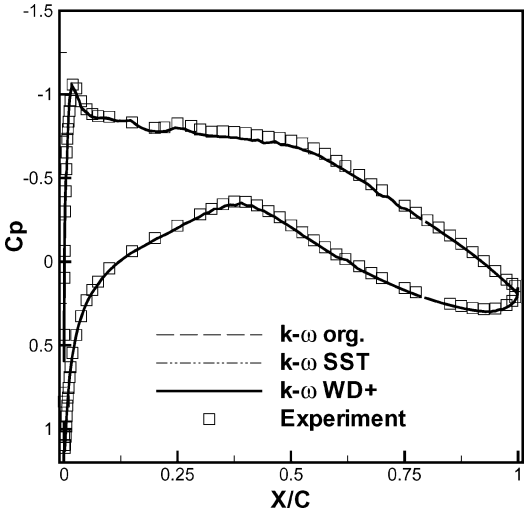

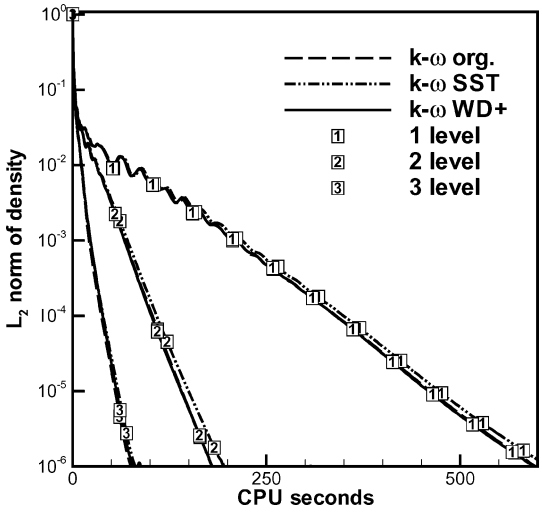

Fig. 2 Wall-pressure coefficient and convergence histories for case 1.

25 after the trailing edge. The grids are stretched far enough from the leading edge to resolve the laminar viscous sublayer. Four sets of grids with different normal wall distances are made in order to perform a grid convergence study, and they are summarized in Table 1.

The computed skin-friction coefficients for three turbulence models are compared with the Blasius solution for the laminar region and Prandtl's $\frac{1}{5}$ law for the turbulent region. The k–ω SST and WD+ models do not display a visible difference for different wall spacings within $y^+ = 4$. However, they cannot predict the transitional behavior[15] for either 8×10^{-6} or 12×10^{-6} (not shown) when Eq. (31) is applied. Applying Eq. (32) can alleviate the grid-spacing limitation of the turbulence models, and an important role of the modification is to increase the value of ω as the grid spacing increases. Figure 1a shows the skin-friction-coefficient distribution for relatively coarse grids when the modified ω value is used. As shown, the grid limitation is reduced for k–ω SST and WD+ models. The modification, however, does not work for the original k–ω model. Figure 1b illustrates the velocity profiles at $X/C = 0.5$ for $\Delta y = 8 \times 10^{-6}$. In the profiles, all models display quite good agreement with the laws of the wall, even when there are three grid points within the viscous sublayer. Equation (32) and the fully turbulent assumption are employed for the following two- and three-dimensional test problems.

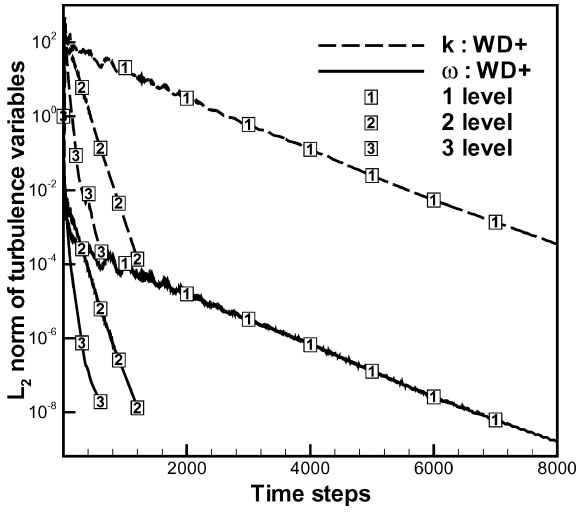

Fig. 3 Convergence histories of k and ω with multigrid level for case 1.

Two-Dimensional Transonic Flows past an RAE2822 Airfoil

The present method is applied to turbulent transonic flows past an RAE2822 airfoil. For a C-type computational grid, the far-field boundary is located at a distance of 20 chord lengths. Four sets

Table 1 Grid systems for turbulent boundary layer

Grid	Size	$\Delta y_{\min} \times 10^6$	y^+
1	193×65	2	$0.6 \sim 0.7$
2	193×65	4	$1.3 \sim 1.4$
3	193×65	8	$2.7 \sim 2.9$
4	193×65	12	$4.1 \sim 4.3$

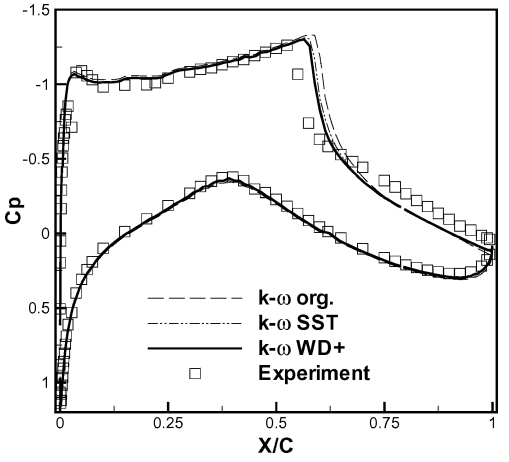

a) Pressure

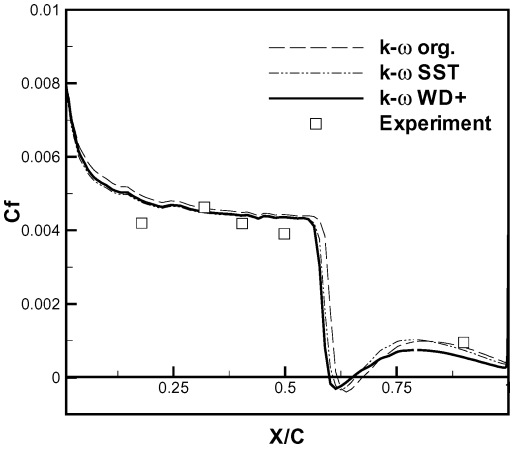

b) Skin friction

Fig. 4 Wall coefficients with turbulence model for case 10.

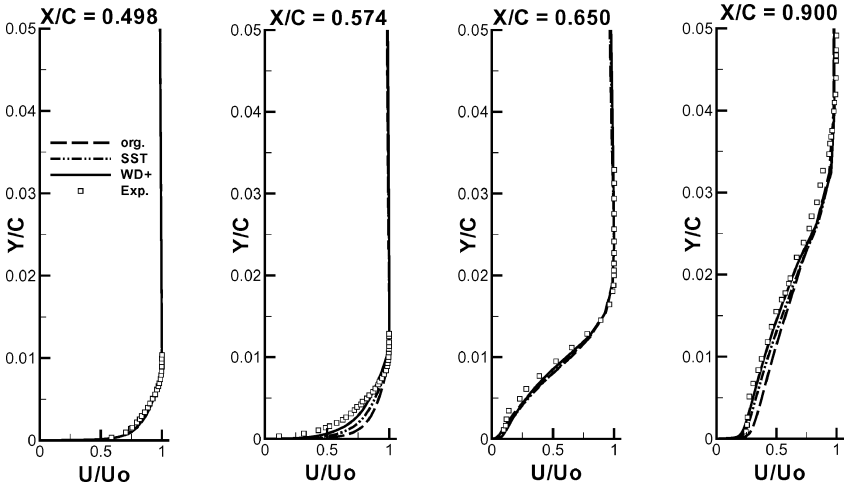

Fig. 5 Velocity profiles on upper surface for case 10.

of grid systems are made to perform the grid test. The finest grid consists of 383 grid points in the flow direction and 65 in the normal direction. The distance to the first cell centers from the wall is 5×10^{-6}, so that y^+ is set below 1. Coarse grids are made by halving the number of node points in the finest grid in each direction. Unless otherwise stated, computations are performed on the finest grid. The experimental data can be found in Ref. 23, and many computational results have been reported for this reference airfoil.[24] Table 2 shows the employed freestream conditions and the corrected incidence angles are the same as those used by Kyle and O'Rourke,[24] whereas transition points are not fixed in this study.

Figure 2 displays the pressure coefficient distribution and convergence historie of each turbulence model for case 1, which represents subcritical unseparated flows. As shown, the computed results of all three models agree well with the experimental data. Computations are performed on a personal computer cluster of four Pentium II 1.4-GHz CPUs. The L_2 norm of the density residual is used for the convergence criterion and it is normalized by the value of the first multigrid iteration. The convergence is also monitored by the aerodynamic coefficients, including lift and drag coefficients, and the solutions are converged to below 0.01% C_L and 0.1% C_D in all test cases. As the multigrid level increases, the number of multigrid cycles decreases. When the L_2 norm is reduced to six orders of magnitude, the three-level multigrid DADI method takes about 80 s (about 380 multigrid cycles), whereas a single grid takes 613 s (6960 cycles) for SST and 595 s (6920) for other methods. The present multigrid reduces the iterations and the computing time to factors of 18 and 7.5, respectively, when compared to the single-grid computation. Convergence histories of the k and ω equations are displayed in Fig. 3 for the k–ω WD+ model. The convergence rate of each

Table 2 Freestream conditions for the test cases

Case	M_∞	$\alpha_{\exp}$	α_{cor}	$Re_c \times 10^{-6}$
1	0.676	2.40	1.93	5.7
10	0.750	3.19	2.81	6.2

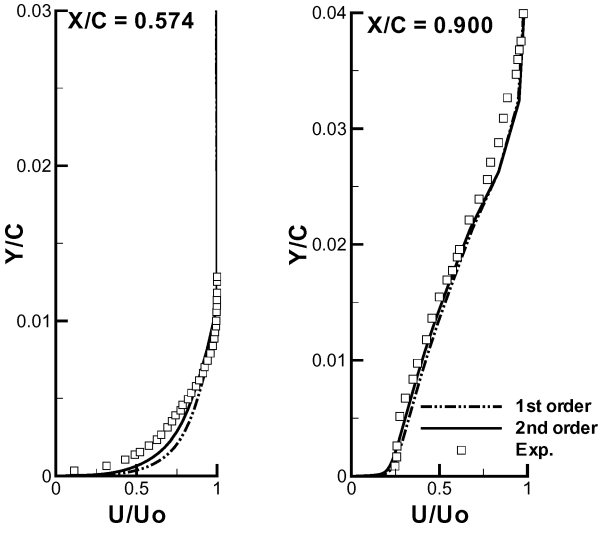

Fig. 6 Velocity profiles with accuracy of spatial discretization.

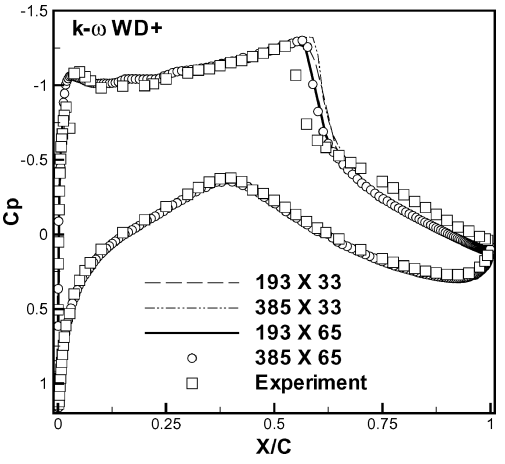

a) Pressure

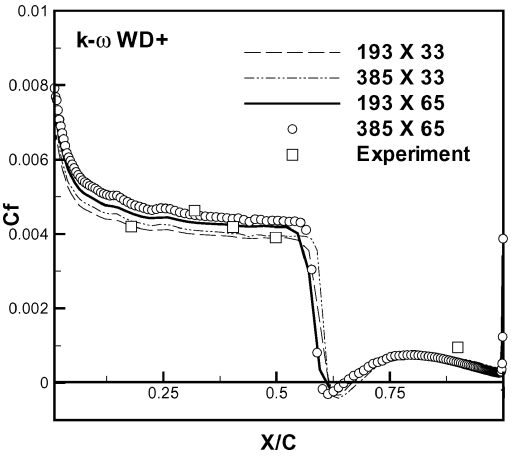

b) Skin friction

Fig. 7 Wall coefficients with grid resolution for case 10.

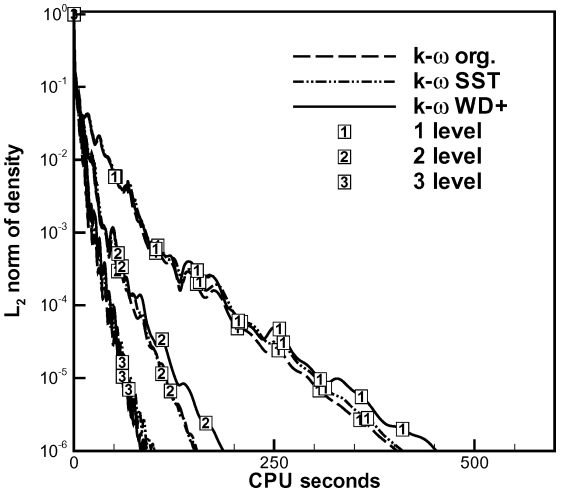

Fig. 8 Convergence histories with multigrid level for case 10.

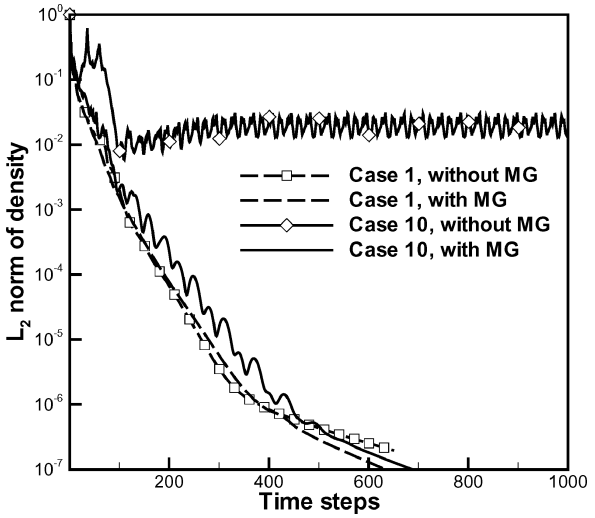

Fig. 9 Convergence histories of the Navier–Stokes equations with and without the multigrid on the turbulence equations.

level is nearly the same as that of the density residual. The original k–ω and SST models have similar convergence trends when compared with the WD+ model. It is noted that the differences in the convergence aspect, as well as the pressure distributions among the turbulence models, are marginal for this unseparated flow.

Case 10 is an example of transonic separated flows. For case 10 with the shock wave/boundary-layer interaction, the SST and WD+ models in Fig. 4 predict the shock aft of the measured location and also yield better agreement with the experimental data than the original k–ω model. All models predict separation to the same extent at different positions, as shown in the skin-friction-coefficient distributions. The velocity profiles on the upper surface in Fig. 5 show that the original k–ω model predicts the smallest separation bubble and the k–ω WD+ model gives the best agreement with experimental profiles. The differences are related to the magnitude of the eddy viscosity in the region of the flow separation. The results show that the weakly nonlinear eddy-viscosity formulation for the k–ω models is superior to the linear formulation in the adverse-pressure-gradient region.

It should also be noted that the turbulence equations are discretized by the second-order MUSCL scheme. Figure 6 illustrates the effect of spatial accuracy on the velocity profiles at $X/C = 0.574$

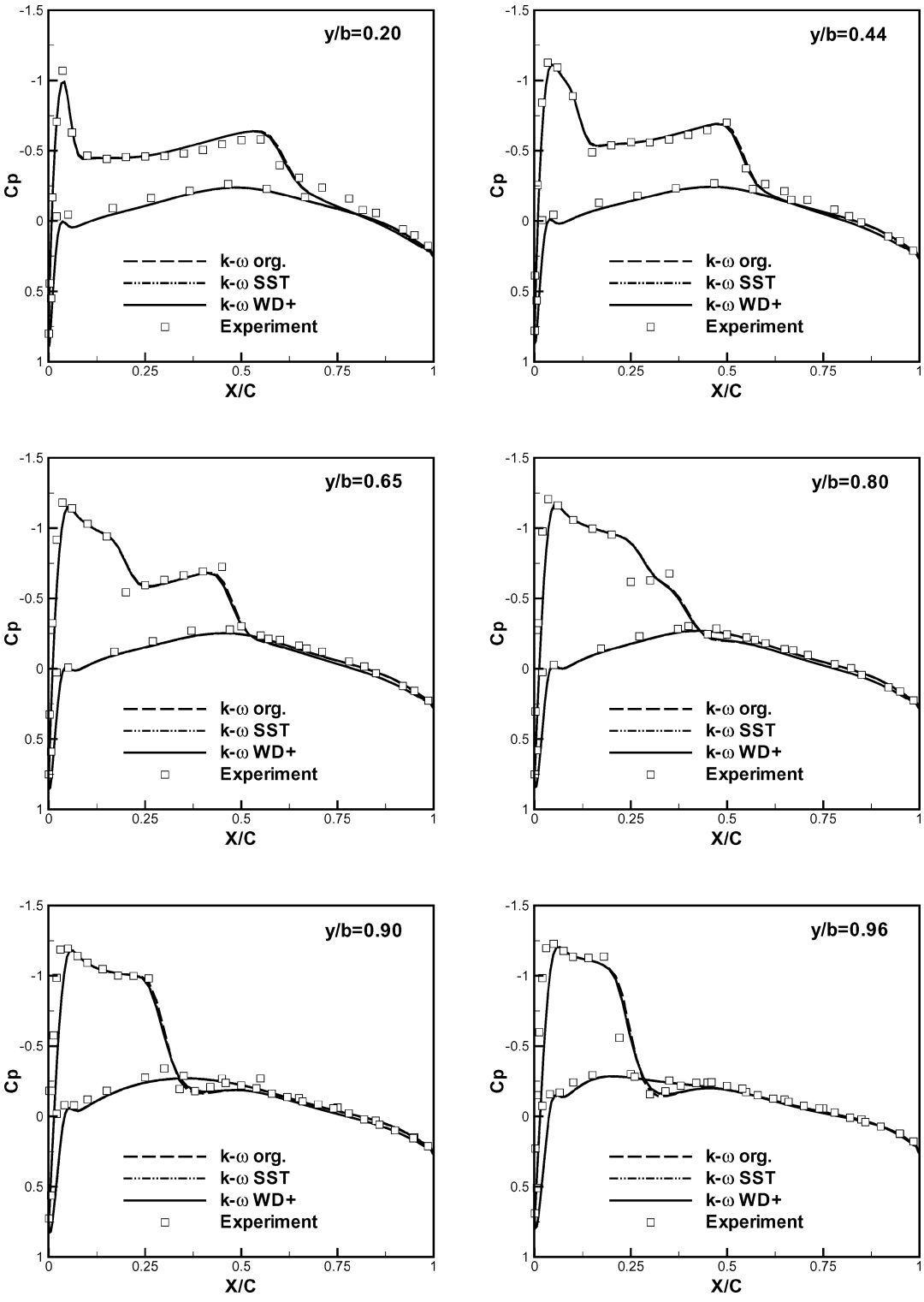

Fig. 10 Wall-pressure coefficients over ONERA-M6 wing at $\alpha = 3.06$ deg.

and 0.900 for case 10. When the second-order scheme for the Navier–Stokes equations is retained and the first-order scheme is used for the turbulence equations, the discrepancies of the velocity profiles from the experimental data are larger than those of the second-order scheme after the shock wave is generated on the upper surface. The difference with spatial discretization is marginal for the pressure distributions (not shown). A grid convergence test using four sets of grids is displayed in Fig. 7 for the k–ω WD+ model. In the skin friction coefficients, an appreciable difference with the grid appears before the shock is generated. Grids finer than the present finest grid give nearly the same pressure and skin-friction distributions. The results show that normal wall spacing is more important in the skin-friction distributions than streamwise spacing. The grid tests of other models are not displayed because they show trends similar to those in the present test case.

Figure 8 shows the convergence for this separated transonic flow. Although a shock wave and separation are generated, the number of iterations and the amount of computing time in the single grid are smaller than those for case 1. By the present multigrid, the iterations and the computing time are reduced by up to factors of 9 and 4, respectively, for all turbulence models when the L_2 norm is reduced to 10^{-6}. Similarly, for case 1, all variables converge with nearly the

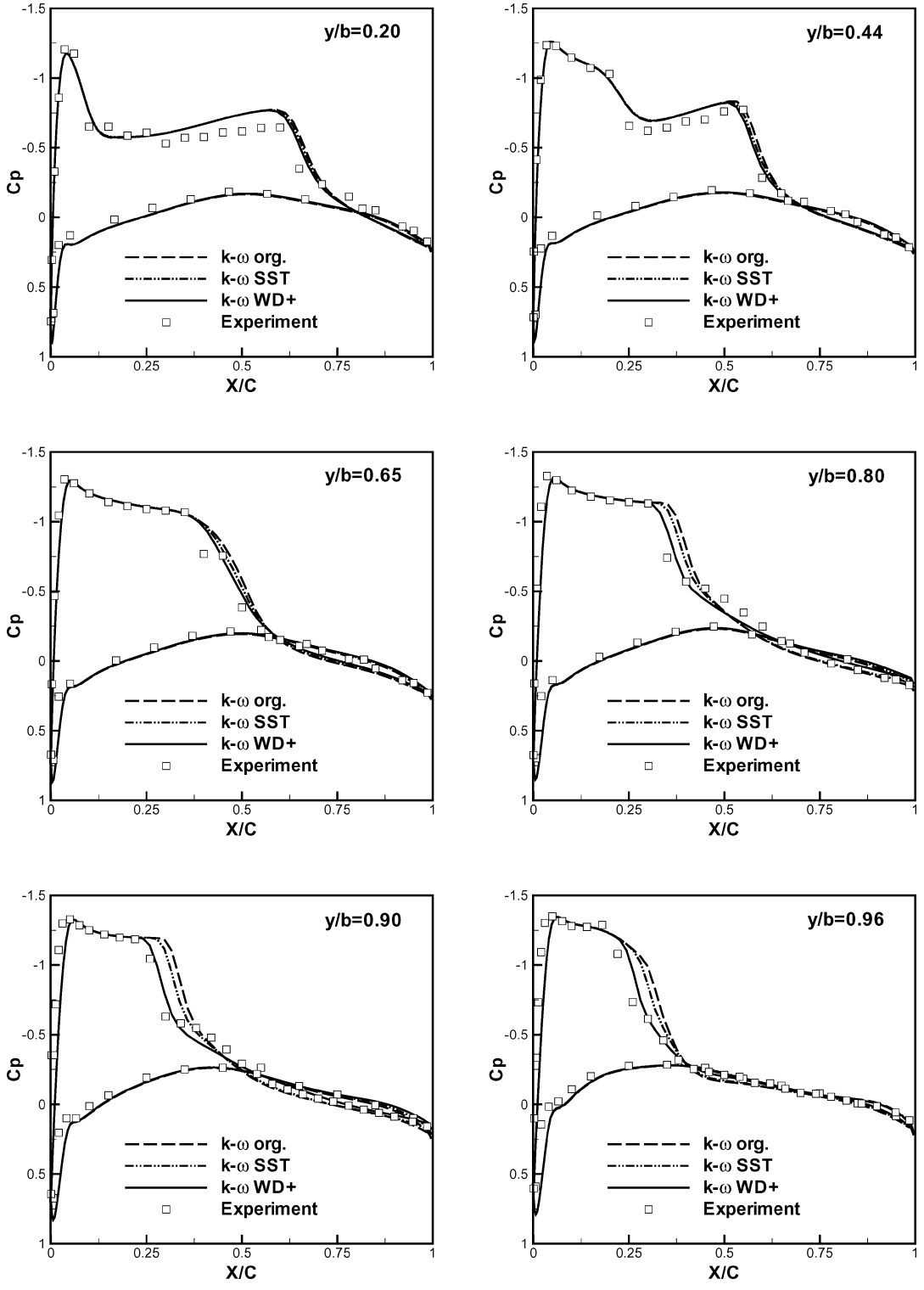

Fig. 11 Wall-pressure coefficients over ONERA-M6 wing at $\alpha = 5.06$ deg.

same convergence rate. Indeed, the convergence histories of the k–ω SST model have severe oscillations after the norm is reduced to 10^{-8} (not displayed). Numerical experiments have shown that fluctuating convergence occurred only when the multigrid method was applied and was caused by the cross-diffusion term of the ω equation. It is believed that special treatments for the cross-diffusion term of the k–ω SST model should be added to the multigrid method.

In the loosely coupled algorithm, the multigrid method can be employed on the Navier–Stokes and turbulence equations separately. Computations without the multigrid on the turbulence equations are performed to examine whether the multigrid method is needed for uncoupled turbulence equations. Figure 9 displays the multigrid convergence of the Navier–Stokes equations with and without the multigrid on the turbulence equations. The solution of the unseparated case 1 converges without difficulty when the multigrid for the turbulence equations is not applied, but the convergence of the turbulence equations is definitely slower than that with the multigrid for the turbulence equations (not shown). The failed convergence without the multigrid for case 10 shows that the multigrid method should be applied to both the Navier–Stokes and turbulence equations, particularly for separated flows.

Three-Dimensional Transonic Flows past an ONERA-M6 Wing

The last test case is a transonic flow past an ONERA-M6 wing. To compare the results for the attached and separated cases, a flow with an angle of attack of 3.06 deg and a Mach number of 0.8395 is selected for the nearly attached flow and one with $\alpha = 5.06$ deg and $M_\infty = 0.8447$ for the separated flow. The freestream Reynolds number is 11.7×10^6. The grid that has been used for validation of CFL3D[25] consists of 149 (streamwise) $\times$49 (normal) $\times$33 (spanwise) grid points. A detailed description of the grid and conditions can be found elsewhere,[25] and the experimental data are available in Ref. 26.

In Figs. 10 and 11, the Cp distributions are compared with the experimental data at each spanwise position. All three models produce nearly the same pressure distributions at $\alpha = 3.06$ deg, but apparent differences at $\alpha = 5.06$ deg are found in the separated region. The k–ω WD+ model gives the best agreement with the experimental data. The difference in the pressure distributions between the WD+ and SST models is more significant for this three-dimensional case than for that of the two-dimensional RAE2822 case 10 with separation. Although stricter confirmation is required, the difference may reflect the different definition of the eddy viscosity and the closure coefficients in the WD+ and SST models.

The convergence histories for these transonic flows are displayed in Figs. 12 and 13. They are plotted with respect to the work unit that corresponds to the computing time for an iteration on a single grid. The computational costs of the original k–ω and WD+ models by using the multigrid are reduced to 21% and 25% of the single grid computations for the unseparated and separated flows, respectively. Although the convergence on the three-level multigrid of the k–ω SST model largely fluctuated for $\alpha = 3.06$ deg, it finally converged at a slow rate. The convergence rates are decreased by approximately five orders of magnitude for the three-level multigrid. This slowdown of the multigrid seems to result from the large grid-aspect ratios and grid stretching.[16] Except for a few convergence problems in the k–ω SST model, the present multigrid algorithm for k–ω models provides good robustness and convergence for the present test cases.

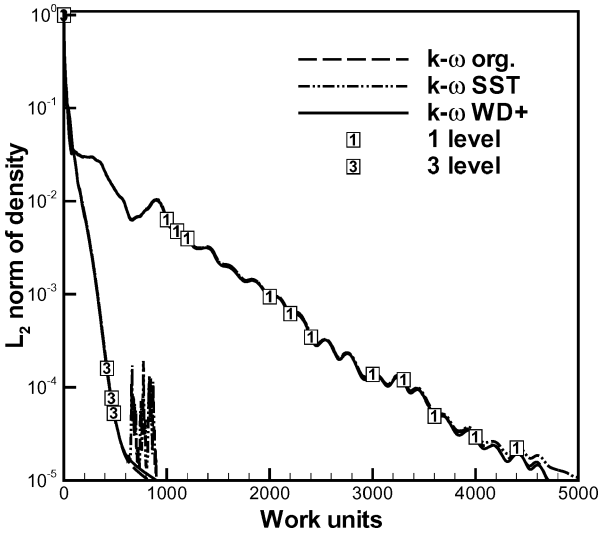

Fig. 12 Convergence histories with turbulence model at $\alpha = 3.06$ deg.

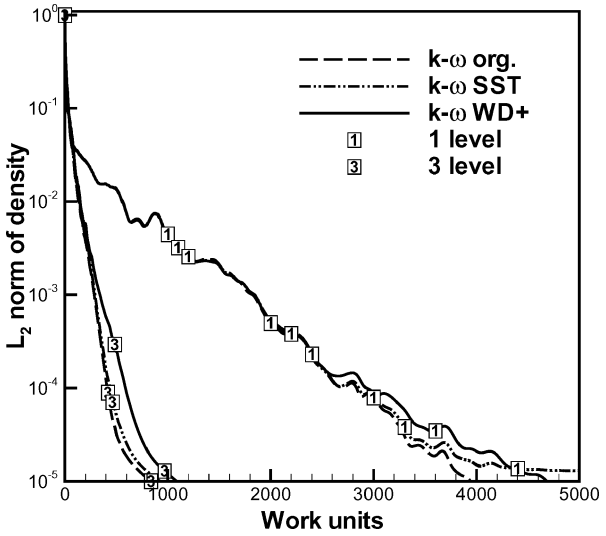

Fig. 13 Convergence histories with turbulence model at $\alpha = 5.06$ deg.

Conclusions

An efficient multigrid DADI method is presented for the Navier–Stokes and k–ω turbulence equations. The Wilcox k–ω, k–ω SST, and WD+ models were implemented by an implicit multigrid method. The equations were solved separately on coarser grids in a loosely coupled fashion. To this end, strongly nonlinear source terms and the eddy viscosity were restricted as frozen variables in the coarser grids. To improve the robustness, the limits for the turbulence variables were simply imposed in the implicit scheme. A grid convergence study over a flat-plate flow was performed, revealing that the WD+ models is less sensitive to normal wall spacing. Numerical results for unseparated and separated transonic flows also showed that the WD+ model using the weakly nonlinear eddy viscosity is in better overall agreement with the experimental data. Numerical results showed that the present freezing and limiting strategies facilitate fast convergence and robust computation of the k–ω turbulence equations. Except for some cases using the SST model, all computations using the multigrid converged well, without any robustness problems, and the present implicit multigrid method was very effective in reducing the amount of computing time.

References

[1]Kolmogorov, A. N., "Equations of Turbulent Motion of an Incompressible Fluid," *Izvestia, Academy of Sciences, USSR, Physics*, Vol. 6, No. 1, 1942, pp. 56–58.

[2]Launder, B. E., and Spalding, D. B., *Mathematical Models of Turbulence*, Academic Press, London, 1972.

[3]Wilcox, D. C., *Turbulence Modeling for CFD*, 2nd ed., DCW Industries, La Canada, CA, 1998.

[4]Wilcox, D. C., "Reassessment of the Scale-Determining Equation for Advanced Turbuulence models," *AIAA Journal*, Vol. 26, No. 11, 1988, pp. 1299–1310.

[5]Menter, F. R., "Influence of Freestream Values on k–ω Turbulence Model Predictions," *AIAA Journal*, Vol. 30, No. 6, 1992, pp. 1657–1659.

[6]Menter, F. R., "Two-Equation Eddy-Viscosity Turbulence Models for Engineering Applications," *AIAA Journal*, Vol. 32, No. 8, 1994, pp. 1598–1605.

[7]Coakley, T. J., "Turbulence Modeling Methods for the Compressible Navier–Stokes Equations," AIAA Paper 83-1693, June 1983.

[8]Bradshaw, P., Ferriss, D. H., and Atwell, N. P., "Calculation of Boundary-Layer Development Using the Turbulent Energy Equation," *Journal of Fluid Mechanics*, Vol. 28, No. 3, 1967, pp. 593–616.
[9]Schumann, U., "Realizability of Reynolds-Stress Turbulence Model," *Physics of Fluids*, Vol. 20, No. 5, 1977, pp. 721–725.
[10]Moore, J. G., and Moore, J., "Realizability in Two-Equation Turbulence Models," AIAA Paper 99-3779, June–July 1999.
[11]Durbin, P. A., "On the k–ϵ Stagnation Point Anomaly," *International Journal of Heat and Fluid Flow*, Vol. 17, No. 1, 1996, pp. 89, 90.
[12]Thivet, F., Knight, D. D., Zheltovodov, A. A., and Maksimov, A. I., "Insights in Turbulence Modeling for Crossing-Shock-Wave/Boundary-Layer Interactions," *AIAA Journal*, Vol. 39, No. 6, 2001, pp. 985–995.
[13]Thivet, F., "Lessons Learned from RANS Simulations of Shock-Wave/Boundary-Layer Interactions," AIAA Paper 2002-0583, Jan. 2002.
[14]Ni, R.-H., "A Multiple-Grid Scheme for Solving the Euler Equations," *AIAA Journal*, Vol. 20, No. 11, 1982, pp. 1565–1571.
[15]Zheng, X., and Liu, F., "Staggered Upwind Method for Solving Navier–Stokes and k–ω Turbulence Model Equations," *AIAA Journal*, Vol. 33, No. 6, 1995, pp. 991–998.
[16]Liu, F., and Zheng, X., "A Strongly Coupled Time-Marching Method for Solving the Navier–Stokes and k–ω Turbulence Model Equations with Multigrid," *Journal of Computational Physics*, Vol. 128, No. 2, 1996, pp. 289–300.
[17]Gerlinger, P., and Brüggemann, D., "Multigrid Convergence Acceleration for Turbulent Supersonic Flows," *International Journal for Numerical Methods in Fluids*, Vol. 24, No. 10, 1997, pp. 1019–1035.
[18]Anderson, W. K., Tomas, J. L., and Van Leer, B., "Comparison of Finite Volume Flux Vector Splittings for the Euler Equations," *AIAA Journal*, Vol. 24, No. 9, 1986, pp. 1453–1460.
[19]Pulliam, T. H., and Chaussee, D. S., "A Diagonal Form of an Implicit Approximate-Factorization Algorithm," *Journal of Computational Physiscs*, Vol. 39, Feb. 1981, pp. 347–363.
[20]Tysinger, T. L., and Caughey, D. A., "Alternating Direction Implicit Methods for the Navier–Stokes Equations," *AIAA Journal*, Vol. 30, No. 8, 1992, pp. 2158–2161.
[21]Caughey, D. A., "Diagonal Implicit Multigrid Algorithm for the Euler Equations," *AIAA Journal*, Vol. 26, No. 7, 1988, pp. 841–851.
[22]Sung, C.-H., Park, S. H., and Kwon, J. H., "Multigrid Diagonalized ADI Method for Compressible Flows," AIAA Paper 2001-2556, June 2001.
[23]Cook, P. H., McDonald, M. A., and Firmin, M. C. P., "Aerofoil RAE2822-Pressure Distributions, and Boundary Layer and Wake Measurements," AGARD, Advisory Rept. 138-A6, May 1979.
[24]Kyle, D. A., and O'Rourke, M. J., "Implementation of Turbulence Models for Shock/Boundary Layer Interaction in Transonic Flow," AIAA Paper 2001-2856, June 2001.
[25]Rumsey, C. L., and Vatsa, V. L., "Comparison of the Predictive Capabilities of Several Turbulence Models," *Journal of Aircraft*, Vol. 32, No. 3, 1995, pp. 510–514.
[26]Schmitt, V., and Charpin, F., "Pressure Distributions on the ONERA-M6-Wing at Transonic Mach Numbers," AGARD, Advisory Rept. 138-B1, May 1979.

R. So
Associate Editor